TTMP vol 2 (2), 2025
doi: 10.30511/TTMP.2025.2057316.1051

Transactions in Theoretical and Mathematical Physics

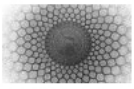

Adaptive numerical optimization for high-fidelity quantum gate control in atom interferometers

Javad Sharifi[1] [a]

[1]Electrical and Computer Engineering Department, Qom University of Technology, Qom, Iran

Received: 07 April 2025 / Accepted: 29 May 2025 / Published: 29 May 2025

Abstract The atomic interferometer has two quantum unitary gates that must be realized for quantum sensing purposes: the atomic gravimeter and the atomic interferometer gyroscope. An optimal cost function that defines the distance between two unitary operators is defined. Based on it, general adaptive (GADA) algorithms for optimization-based quantum control are innovated to realize the atomic mirror and beam-splitter gates. We used optimal quantum control to realize those atom interferometer gates. We obtained gate fidelities of 0.99980 and 0.99998 for the mirror and the beam-splitter gates, respectively. In this research, a two-level atom system with clock transitions $^1S_0 \leftrightarrow {}^3P_0$ of strontium(^{87}Sr) atom was employed.

1 Introduction

Atoms are surprisingly accurate measurement devices. They can detect external signals with high sensitivity; furthermore, they are employed for very accurate time measurement in atomic clocks. An important class of atom sensors are atom interferometers that in a controlled manner have been versatilized for investigation fundamental physics such as particle physics, general relativity [1], gravity [2, 3], gravitational wave detection [4, 5], dark matter [6] and cosmology. Atom interferometers also have several applications in quantum sensing and quantum metrology, navigation, and geophysics. Zhaoshan long-baseline atom interferometer gravitation antenna (ZAIGA) in China [7] and MAGIS-100 atom interferometer in Fermilab in USA [5] are among the most famous. For the detailed formulation of atom interferometry, see the lecture [8]. Atomic interferometer gyroscopes are more accurate than optical gyroscopes, and shortly, they are hoped to become more accurate than mechanical gyroscopes. Atom interferometers are more angle-sensitive than light interferometers because the de Broglie wavelength is much smaller than optical wavelengths. Hence, when covering the same area, the two types of interferometers display differences in phase shifts. Atom interferometers cause much longer phase shifts based on the Sagnac phase shift formula [9, 10].

Moreover, the precise working of any technology depends on its embedded control system, and especially, quantum technology requires the implementation of arbitrary control operations on the quantum system [11]. Among different technologies, quantum technology will become a dominant future technology that will change the whole lives of human beings. For quantum technology, it is essential to develop quantum materials, devices, and circuits; then, we must precisely engineer and control quantum states or unitary gates of such devices based on appropriate high-fidelity circuit readout. For example, for quantum computing applications, the exact unitary matrix of quantum gates must be implemented despite decoherence, relaxation, and, in some quantum materials, leakage errors, which lead to quantum computational subspace exit from qubit computational subspace. All of these issues, in addition to the development and engineering of the quantum devices, need precise and high-fidelity quantum control protocols [12–16] to be implemented on appropriate classical hardware such as SOC-FPGA and the quantum hardware. Quantum control as an essential part of the development of quantum science and technology dates back to 1980-2000 by pioneering research works in [17–20]. Optimized control, especially numerical pulse-based optimal control, performs better than the other quantum control methods since it guarantees optimal realization and increased convergence speed to achieve the desired quantum gates or states. Numerical optimizations were at the centre of researchers' attention. They included stochastic gradient descent [21], adaptive gradient [22, 23], momentum method [24], adaptive momentum [25],

[a]jv.sharifi@gmail.com

Levenberg-Marquardt [26], adaptive delta [27], etc. These methods have been successful in different scientific and engineering applications.

In this research, we initially innovated a numerical optimal control method. Then, we introduced the quantum dynamics of a two-level atomic transition clock and the atom interferometer. We introduced the cost function for gate realization, which was adopted from the related quantum information literature and derived the numerical pulse optimal control for this atomic system. Finally, we numerically simulated the optimal control for implementing two unitary gates of the atom interferometer, i.e., the atomic reflection or mirror and the atomic beam-splitter gate.

2 Optimal Control Methodology

Lets start with a cost function $J\big(\underline{u}(t)\big)$ of the control vector $\underline{u}_{p\times 1}(t)$. We denote the gradient vector of this cost as $\underline{g}(t) = \frac{\partial J}{\partial \underline{u}(t)}$ and the Hessian matrix as $S_{p\times p}(t) = \frac{\partial \underline{g}(t)}{\partial \underline{u}(t)}$. Now, let us expand the Taylor series of this cost function around the control vector as:

$$J\big(\underline{u}(t)+\Delta\underline{u}(t)\big) = J\big(\underline{u}(t)\big) + \Delta\underline{u}(t)^T\underline{g}(t) + \frac{1}{2}\Delta\underline{u}(t)^T S(t)\Delta\underline{u}(t) + \text{h.o.t.} \quad (1)$$

We consider the first three terms of this optimization. To minimize the cost function, the future values of the cost must be less than those of its previous ones; hence, $J\big(\underline{u}(t)+\Delta\underline{u}(t)\big) < J\big(\underline{u}(t)\big)$ leads to:

$$\Delta\underline{u}(t)^T.\Big(\underline{g}(t)+\frac{1}{2}S(t)\Delta\underline{u}(t)\Big) < 0. \quad (2)$$

Employing the above inner product, a solution of this inequality is $\underline{g}(t)+\frac{1}{2}S(t)\Delta\underline{u}(t) = -\lambda\Delta\underline{u}(t)$ in which $\lambda > 0$ is a free positive parameter. Then by simplifying this relation, we will obtain $\Delta\underline{u} = -\big(\lambda I+\frac{1}{2}S\big)^{-1}\underline{g}$ and then, we would have the following numerical control vector at iteration $k \equiv k\delta t$:

$$\underline{u}_{k+1} = \underline{u}_k - \big(\lambda I+\frac{1}{2}S_k\big)^{-1}\underline{g}_k. \quad (3)$$

Let us convert the control vector in Eq. 3 to adaptive. Then the following general adaptive (GADA) optimization would be obtained:

$$\begin{aligned}
&\underline{\xi}_k = \beta_1\underline{\xi}_{k-1} + \gamma_1\underline{g}_k \quad , \quad \underline{\xi}_0 = \underline{0}_{p\times 1},\\
&M_k = \beta_2 M_{k-1} + \gamma_2 S_k \quad , \quad M_0 = [0]_{p\times p},\\
&\underline{u}_{k+1} = \underline{u}_k - \eta\big(M_k+\lambda I\big)^{-1}\underline{\xi}_k.
\end{aligned} \quad (4)$$

In the above equation, $\underline{g}_k \to \underline{\xi}_k$ and $S_k \to M_k$ are one-order discrete-time dynamic systems without any transfer function zero; however, they have transfer function poles at β_1, β_2, Note that the pole of $S_k \to M_k$ is the zero of $\underline{\xi}_k \to \underline{u}_k$ and then it can be outside of unit-circle and the pole of $\underline{g}_k \to \underline{\xi}_k$ is the pole of $\underline{\xi}_k \to \underline{u}_k$. Then to stabilize the control signal iteration $\beta_1 \in [0,1)$ and $\beta_2 \in R$ and the parameters γ_1, γ_2 must be real numbers. Actually, with this adaptation, we include a forgetting factor coefficient of gradient vectors and Hessian matrices in optimization-based control, i.e. $M_k = \gamma_2\sum_{i=1}^{k}(\beta_2^{k-i}H_i), \underline{\xi}_k = \gamma_1\sum_{i=1}^{k}(\beta_1^{k-i}\underline{g}_i)$, then by adding the momentum terms and the Hessian matrix and gradient vector became dynamic which causes the optimal control system to converge faster compared to the conventional gradient optimization methods. We mention that this adaptive optimization for $\beta_1 = \beta_2 = \gamma_2 = 0, \gamma_1 = 1, \lambda = 1$ diminishes to the stochastic gradient descent (SGD). For parameters $\beta_1 = \beta_2 = 0, \gamma_1 = 1$ and a quadratic cost function, GADA diminishes to the Levenberg–Marquardt (LM) optimization, and for $\beta_2 = \gamma_2 = 0$ it diminishes to adaptive gradient method (AdaGrad). Note that SGD and LM are not adaptive optimization methods. If the inversion of matrix in equation4 for the large Hessian matrix is problematic, heuristically we can consider only the diagonal elements of the Hessian matrix S_k and the off-diagonal elements equal to zero,i.e. $S_k = \text{diag}\big(\frac{\partial^2 J}{\partial u_{1,k}^2},..,\frac{\partial^2 J}{\partial u_{p,k}^2}\big)$. In this condition, the M_k matrix and also the $M_k+\lambda I$ are always diagonal and the inverse $(M_k+\lambda I)^{-1}$ is trivial, let us call this simplified adaptive optimization, the diagonal adaptive (DADA) algorithm in the subsequent sections.

3 Atom Interferometer Application

3.1 Two-Level Atom Rabi Oscillation as Rotation over Bloch Sphere

These quantum mechanical matter waves can be manipulated with the atomic equivalents of lenses, beam-splitters, and mirrors. Atom interferometry is analogous to optical interferometry. In both interferometers, a beam-splitter splits an incident wave into two paths. The two paths are later redirected back toward each other with mirrors and overlapped on a final beam-splitter to produce an interference pattern (see figure 1). Making beam-splitters and mirrors in

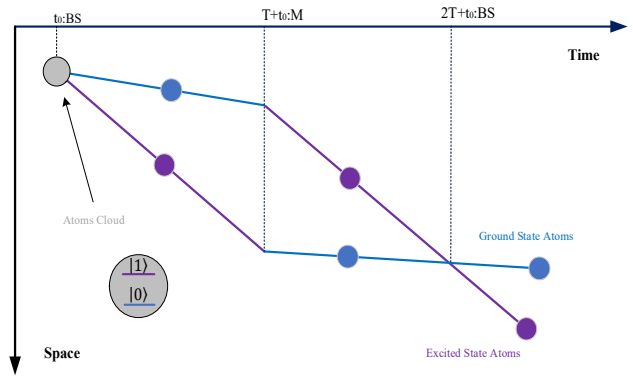

Fig. 1 Mach-Zehnder based Atom Interferometer in space-time coordinate: At times t_0 and $2T+t_0$, the atomic beam splitter (BS) and also at time $T+t_0$, the atomic mirror (M) must be implemented.

optical beams is known. To implement similar interferometer devices, such as those in atomic experiments, an ensemble of cold two-level atoms such as Strontium atom (^{87}Sr) in clock transition states ($|0\rangle = {}^1S_0 \leftrightarrow |1\rangle = {}^3P_0$) with a $\lambda_{|0\rangle\leftrightarrow|1\rangle} = 698$nm wavelength transition and a very long coherence time is considered. Freely falling atoms have enabled the development of atomic gravimeters and atomic gyrometers. In these devices, an atom cloud measures acceleration by sensing the spatial phase shift of a laser beam along its freely falling trajectory.

The quantum system described by Schrödinger equation as ($\hbar \equiv 1$): $i\frac{d}{dt}|\psi_t\rangle = H(t)|\psi_t\rangle$. The Hamiltonian of two-level atom in Rabi modeling is:

$$H(t) = \frac{1}{2}\begin{pmatrix} \Delta(t) & \Omega(t)e^{-i\phi} \\ \Omega(t)e^{i\phi} & -\Delta(t) \end{pmatrix}, \tag{5}$$

in which Ω, Δ are Rabi frequency and detuning respectively and ϕ is the initial phase of laser electric field. Sometimes, scientists employ the three-level Raman transition atoms for atom interferometer [8]; in this case, there are two stable atomic levels $|0\rangle, |1\rangle$ and an unstable excited state $|e\rangle$. For Raman's levels atoms, there are two laser beams; one is the upward beam with Rabi frequency Ω_1 and phase ϕ_1, which transfers the atomic state transition $|0\rangle \to |e\rangle$ and the other is a downward beam with Rabi frequency Ω_2 and phase ϕ_2 which lead to transition $|e\rangle \to |1\rangle$, the detuning in both transitions assumes to be approximately equal to Δ. In [28] it is shown that with two Rabi-frequencies Ω_1, Ω_2, the three-level Raman transition atom can be approximated with two-level atom with $\Omega = \frac{\Omega_1\Omega_2}{2\Delta}, \phi = \phi_2 - \phi_1$, then for every interferometer, we can use two-level Hamiltonian model of equation5. We can write this Hamiltonian based on Pauli matrices $\sigma_x, \sigma_y, \sigma_z$ as follows:

$$H(t) = \frac{1}{2}\Big(\Omega(t)\cos(\phi)\sigma_x + \Omega(t)\sin(\phi)\sigma_y + \Delta(t)\sigma_z\Big). \tag{6}$$

Let us define the infinitesimal evolution as $\mathscr{M}_n = e^{-iH_n\delta t}$, then the unitary propagator at time step $k\delta t$ is:

$$U_k = \mathscr{M}_k\mathscr{M}_{k-1}....\mathscr{M}_1 \quad , \quad |\psi_k\rangle = U_k|\psi_0\rangle. \tag{7}$$

The evolution of the two-level atom at time sample $t = k\delta t$ is:

$$\mathscr{M}(n\delta t) = \exp\Big(-\tfrac{i}{2}\delta t\big(\cos(\phi)\sigma_x + \sin(\phi)\sigma_y\big)\Omega(n\delta t) - \tfrac{i}{2}\delta t\,\sigma_z\Delta(n\delta t)\Big). \tag{8}$$

We know that, the rotation operator is [29]:

$$\begin{aligned}\mathscr{R}_{\vec{r}(t),\alpha(t)} &= e^{-i\frac{\alpha(t)}{2}\hat{r}(t)\cdot\vec{\sigma}} \\ &= \sin\big(\tfrac{1}{2}\alpha(t)\big)I - i\cos\big(\tfrac{1}{2}\alpha(t)\big)\,\hat{r}(t)\cdot\vec{\sigma},\end{aligned} \tag{9}$$

where $\vec{\sigma} = \sigma_x\hat{x} + \sigma_y\hat{y} + \sigma_z\hat{z}$, and $\hat{r} = r_x\hat{x} + r_y\hat{y} + r_z\hat{z}$ is the rotation axis and $\alpha = \omega_q t$ is the rotation angle, ω_q is the angular speed of quantum state vector on Bloch sphere. By comparing Eq. (8) and Eq.(9), we will obtain:

$$\alpha\hat{r} = \delta t\Big(\cos(\phi)\,\Omega(n\delta t)\,\hat{x} + \sin(\phi)\,\Omega(n\delta t)\,\hat{y} + \Delta(n\delta t)\,\hat{z}\Big). \tag{10}$$

Then since $|\alpha\hat{r}| = \alpha$ we obtain:

$$\alpha(n\delta t) = \delta t\sqrt{\Omega_n^2 + \Delta_n^2}, \tag{11}$$

$$\hat{r}(n\delta t) = \cos(\phi)\frac{\Omega_n}{\sqrt{\Omega_n^2+\Delta_n^2}}\hat{x} + \sin(\phi)\frac{\Omega_n}{\sqrt{\Omega_n^2+\Delta_n^2}}\hat{y} + \frac{\Delta_n}{\sqrt{\Omega_n^2+\Delta_n^2}}\hat{z}. \tag{12}$$

In these relations, we use these abbreviations $\Omega_n = \Omega(n\delta t)$, $\Delta_n = \Delta(n\delta t)$.

3.2 Atom Interferometer Gates Realization

The unitary operator of a mirror (M) and beam-splitter (BS) is:

$$U_M = \begin{pmatrix} 0 & 1 \\ 1 & 0 \end{pmatrix} = \sigma_x, U_{BS} = \frac{1}{\sqrt{2}} \begin{pmatrix} 1 & i \\ i & 1 \end{pmatrix}. \tag{13}$$

The aim of gate optimization is the implementation of atomic unitary operator of Eq. (7) to move to the desired gate of Eq. (13). For this aim, we can select an objective function as:

$$\begin{aligned} J_{\text{gate}}(T) &:= 1 - \frac{1}{d^2} \left| \langle U_{\text{gate}}, U_{\text{atom}}(T) \rangle \right|^2 \\ &= 1 - \frac{1}{d^2} \left| \text{Tr}\left(U_{\text{gate}}^{\dagger} U_{\text{atom}}(T) \right) \right|^2, \end{aligned} \tag{14}$$

in which $U_{atom} = U(k\delta t), gate = M, BS, d = \dim(U_{gate}) = 2$ and † is transpose complex conjugate. For this cost function as $U_{atom} \to U_{gate}$ then $J_{gate} \to 0$. The control vector includes Rabi-frequency and detuning, then the gradient vector and the Hessian matrix are:

$$\underline{u}_k = \begin{bmatrix} \Omega_k \\ \Delta_k \end{bmatrix}, \ \underline{g}_k = \begin{bmatrix} \frac{\partial J_{gate}}{\partial \Omega_k} \\ \frac{\partial J_{gate}}{\partial \Delta_k} \end{bmatrix}, \ S_k = \begin{pmatrix} \frac{\partial^2 J_{gate}}{\partial \Omega_k^2} & \frac{\partial^2 J_{gate}}{\partial \Omega_k \partial \Delta_k} \\ \frac{\partial^2 J_{gate}}{\partial \Delta_k \partial \Omega_k} & \frac{\partial^2 J_{gate}}{\partial \Delta_k^2} \end{pmatrix}. \tag{15}$$

3.3 Code Structure and Parameter Selection

For simulation, we develop the codes in Python 3 by using Numpy, QuTip, and Matplotlib packages. The general learning parameter η is set to 10^8, and the other parameters for each gate realization are explained in subsequent subsections. After setting the parameters, we optimize them in each iteration in a for loop based on the above adaptive optimization. In the for loop, we save each quantum state and fidelity value, which allows us to plot the quantum state transition on the Bloch sphere and also the fidelity curve.

3.4 Mirror Gate

At first we choose to implement the mirror gates, then we will obtain the following cost function:

$$\begin{aligned} J_M &= 1 - \cos^2\left(\tfrac{1}{2}\alpha\right) r_x^2 \\ &= 1 - \cos^2(\phi)\cos^2\left(\tfrac{1}{2}\delta t \sqrt{\Omega_n^2 + \Delta_n^2}\right) \frac{\Omega_n^2}{\Omega_n^2 + \Delta_n^2}. \end{aligned} \tag{16}$$

Then, the following updates for the gradient vector will be obtained:

$$\begin{aligned} \frac{\partial J_M}{\partial \Omega_k} &= \tfrac{1}{2}\delta t \cos^2(\phi)\sin(\alpha) \frac{\Omega_k^3}{\left(\Omega_k^2 + \Delta_k^2\right)^{3/2}} \\ &\quad - 2\cos^2(\phi)\cos^2\left(\tfrac{1}{2}\alpha\right) \frac{\Omega_k \Delta_k^2}{\left(\Omega_k^2 + \Delta_k^2\right)^2}, \end{aligned} \tag{17}$$

$$\begin{aligned} \frac{\partial J_M}{\partial \Delta_k} &= \tfrac{1}{2}\delta t \cos^2(\phi)\sin(\alpha) \frac{\Delta_k \Omega_k^2}{\left(\Omega_k^2 + \Delta_k^2\right)^{3/2}} \\ &\quad + 2\cos^2(\phi)\cos^2\left(\tfrac{1}{2}\alpha\right) \frac{\Delta_k \Omega_k^2}{\left(\Omega_k^2 + \Delta_k^2\right)^2}. \end{aligned} \tag{18}$$

The elements of Hessian matrix by neglecting $(\delta t)^2$ term is:

$$\begin{aligned} \frac{\partial^2 J_M}{\partial \Omega_k^2} &= \tfrac{5}{2}\delta t \cos^2(\phi)\sin(\alpha) \frac{\Omega_k^2 \Delta_k^2}{(\Omega_k^2 + \Delta_k^2)^{5/2}} \\ &\quad - 2\cos^2(\phi)\cos^2\left(\tfrac{1}{2}\alpha\right) \Delta_k^2 \frac{\Delta_k^2 - 3\Omega_k^2}{(\Omega_k^2 + \Delta_k^2)^3}, \end{aligned} \tag{19}$$

$$\begin{aligned} \frac{\partial^2 J_M}{\partial \Delta_k^2} &= \tfrac{1}{2}\delta t \cos^2(\phi)\sin(\alpha)\, \Omega_k^2 \frac{\Omega_k^2 - 4\Delta_k^2}{(\Omega_k^2 + \Delta_k^2)^{5/2}} \\ &\quad + 2\cos^2(\phi)\cos^2\left(\tfrac{1}{2}\alpha\right) \Omega_k^2 \frac{\Omega_k^2 - 3\Delta_k^2}{(\Omega_k^2 + \Delta_k^2)^3}, \end{aligned} \tag{20}$$

$$\begin{aligned} \frac{\partial^2 J_M}{\partial \Omega_k \partial \Delta_k} &= \frac{\partial^2 J_M}{\partial \Delta_k \partial \Omega_k} \\ &= \tfrac{1}{2}\delta t \cos^2(\phi)\sin(\alpha) \frac{2\Omega_k \Delta_k^3 - 3\Delta_k \Omega_k^3}{(\Omega_k^2 + \Delta_k^2)^{5/2}} \\ &\quad - 4\cos^2(\phi)\cos^2\left(\tfrac{1}{2}\alpha\right) \frac{\Omega_k^3 \Delta_k - \Omega_k \Delta_k^3}{(\Omega_k^2 + \Delta_k^2)^3}. \end{aligned} \tag{21}$$

To make Optimization possible, we must have the initial phase of the Rabi signal as $\phi \neq \frac{(2n+1)\pi}{2}$. Based on SGD with parameter setting of $(\beta_1 = \beta_2 = \gamma_2 = 0, \gamma_1 = 0.85, \lambda = 1)$ in GADA method, the optimal control signals are depicted in figure (2 a_1, b_1) and the fidelity of gate optimization is depicted in figure (2 c_1). Also, with the GADA method, the optimal control signals are depicted in figure (2 a_2, b_2) and the fidelity of gate optimization is depicted in figure (2 c_2). By using the GADA optimal control, after 44 samples of 1-microsecond control pulses (see table 1), we obtain gate

fidelity of 0.999 for the atomic mirror realization, which has a unitary of atomic gate approximately up to a phase factor $e^{i\frac{\pi}{2}}$ which is different from the actual mirror gate of Eq. 13:

$$U_{\text{atomM}}(N\delta t) = \begin{pmatrix} 0.02-0.06i & 0.999i \\ 0.999i & 0.02+0.06i \end{pmatrix}, \quad N = 44, \quad \delta t = 1\,\mu\text{s}. \tag{22}$$

By gate optimization, simultaneously we can control two populations of atoms, one population from state $|0\rangle$ to $|1\rangle$ and the other population from $|1\rangle$ to $|0\rangle$ as we can see in figure (2 d_1) for SGD and figure (2 d_2) for GADA method. Since the result of SGD,LM and AdaGrad are similar to each other and also GADA is similar to DADA, then one method from each set is depicted in figure 2.

Table 1 Number of control pulses ($\delta t = 1\,\mu$s each pulse width) and fidelity based on optimization method to realize NOT gate

Optimization Method	Control Pulse Number	NOT Gate Fidelity
SGD	42	0.99850
AdaGrad	45	0.99846
LM	43	0.99936
GADA	44	0.99980
DADA	44	0.99990

3.5 Beam-Splitter Gate

Now, to optimally implement the atomic beam-splitter on atomic clouds, we will optimize the following cost function:

$$J_{BS} = 1 - \frac{1}{2}\left(\sin(\tfrac{1}{2}\alpha) - \cos(\tfrac{1}{2}\alpha) r_x\right)^2, \tag{23}$$

and after simple calculations, we will have the following update rules for Rabi frequency and detunings:

$$\frac{\partial J_{BS}}{\partial \Omega_k} = -\left(\sin\left(\tfrac{1}{2}\alpha\right) - \cos\left(\tfrac{1}{2}\alpha\right) r_x\right) \times \left(\tfrac{1}{2}\delta t \left(\cos\left(\tfrac{1}{2}\alpha\right) + \sin\left(\tfrac{1}{2}\alpha\right) r_x\right) \frac{\Omega_k}{\sqrt{\Omega_k^2+\Delta_k^2}} - \cos\left(\tfrac{1}{2}\alpha\right)\cos(\phi)\frac{\Delta_k^2}{\left(\Omega_k^2+\Delta_k^2\right)^{3/2}}\right), \tag{24}$$

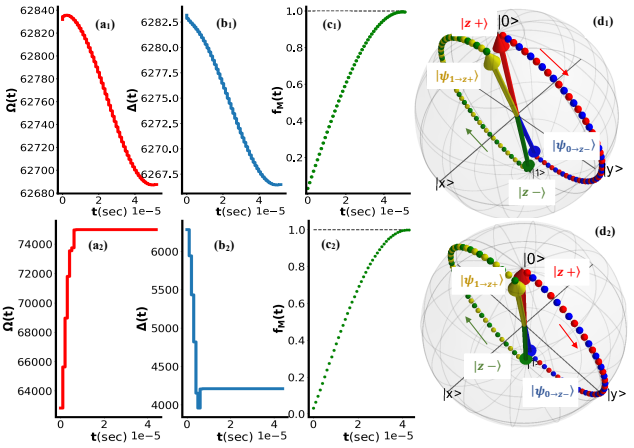

Fig. 2 Atom interferometer mirror gate realization: Top is for SGD and Bottom is for GADA based on optimal quantum control methods. SGD parameters: ($\beta_1 = \beta_2 = \gamma_2 = 0, \gamma_1 = 1, \lambda = 1$) and GADA parameters ($\beta_1 = 0.85, \beta_2 = 85, \gamma_1 = \gamma_2 = 1, \lambda = 10^{-2}$). ($a_1, b_1$) are the control pulses and (c_1) fidelity function for implementation of the atomic mirror gate realization and (d_1) shows the simultaneous quantum state transfer ($|0\rangle = |z+\rangle \to |1\rangle = |\psi_{0\to z-}\rangle$ and $|1\rangle = |z+\rangle \to |0\rangle = |\psi_{1\to z+}\rangle$) on Bloch-sphere using optimal mirror gate realization with SGD. Figures (a_2, b_2, c_2) are the control pulses and the fidelity over time for mirror implementation with GADA. (d_2) displays simultaneous quantum state transfer using optimal mirror gate realization on Bloch-sphere via GADA.

$$\frac{\partial J_{BS}}{\partial \Delta_k} = -\left(\sin\left(\tfrac{1}{2}\alpha\right) - \cos\left(\tfrac{1}{2}\alpha\right) r_x\right) \times \left(\tfrac{1}{2}\delta t \left(\cos\left(\tfrac{1}{2}\alpha\right) + \sin\left(\tfrac{1}{2}\alpha\right) r_x\right) \frac{\Delta_k}{\sqrt{\Omega_k^2+\Delta_k^2}} + \cos\left(\tfrac{1}{2}\alpha\right)\cos(\phi)\frac{\Delta_k\Omega_k}{\left(\Omega_k^2+\Delta_k^2\right)^{3/2}}\right), \tag{25}$$

and the Hessian matrix elements are:

$$\begin{aligned}\frac{\partial^2 J_{BS}}{\partial \Omega_k^2} = &-\left(\tfrac{1}{2}\delta t \left(\cos\left(\tfrac{1}{2}\alpha\right) + \sin\left(\tfrac{1}{2}\alpha\right) r_x\right) \frac{\Omega_k}{\sqrt{\Omega_k^2+\Delta_k^2}} - \cos\left(\tfrac{1}{2}\alpha\right)\cos(\phi)\frac{\Delta_k^2}{\left(\Omega_k^2+s_\Delta^2\right)^{3/2}}\right)^2 \\ &- \left(\sin\left(\tfrac{1}{2}\alpha\right) - \cos\left(\tfrac{1}{2}\alpha\right) r_x\right) \times \left[\tfrac{1}{2}\delta t \sin\left(\tfrac{1}{2}\alpha\right) \frac{\Omega_k\Delta_k^2}{\Omega_k^2+\Delta_k^2} + \tfrac{1}{2}\delta t \left(\cos\left(\tfrac{1}{2}\alpha\right) + \sin\left(\tfrac{1}{2}\alpha\right) r_x\right) \frac{\Delta_k^2}{\left(\Omega_k^2+\Delta_k^2\right)^{3/2}} \right. \\ &\left. + \tfrac{1}{2}\delta t \sin\left(\tfrac{1}{2}\alpha\right)\cos(\phi)\frac{\Delta_k^2\Omega_k}{\left(\Omega_k^2+\Delta_k^2\right)^2} + 3\cos\left(\tfrac{1}{2}\alpha\right)\cos(\phi)\frac{\Delta_k^2\Omega_k}{\left(\Omega_k^2+\Delta_k^2\right)^3}\right],\end{aligned} \tag{26}$$

$$\frac{\partial^2 J_{BS}}{\partial \Delta_k^2} = -\Bigg(\tfrac{1}{2}\delta t \left(\cos\left(\tfrac{1}{2}\alpha\right) + \sin\left(\tfrac{1}{2}\alpha\right) r_x\right) \frac{\Delta_k}{\sqrt{\Omega_k^2+\Delta_k^2}} + \cos\left(\tfrac{1}{2}\alpha\right)\cos(\phi)\frac{\Delta_k\Omega_k}{\left(\Omega_k^2+\Delta_k^2\right)^{3/2}}\Bigg)^2 - \left(\sin\left(\tfrac{1}{2}\alpha\right) - \cos\left(\tfrac{1}{2}\alpha\right) r_x\right) \times \Bigg[- \tfrac{1}{2}\delta t \sin\left(\tfrac{1}{2}\alpha\right)\frac{\Omega_k^2\Delta_k}{\Omega_k^2+\Delta_k^2} + \tfrac{1}{2}\delta t \left(\cos\left(\tfrac{1}{2}\alpha\right) + \sin\left(\tfrac{1}{2}\alpha\right) r_x\right)\frac{\Omega_k^2}{\left(\Omega_k^2+\Delta_k^2\right)^{3/2}} - \tfrac{1}{2}\delta t \sin\left(\tfrac{1}{2}\alpha\right)\cos(\phi)\frac{\Delta_k^2\Omega_k}{\left(\Omega_k^2+\Delta_k^2\right)^2} + \cos\left(\tfrac{1}{2}\alpha\right)\cos(\phi)\frac{\Omega_k^3-2\Delta_k^2\Omega_k}{\left(\Omega_k^2+\Delta_k^2\right)^{5/2}}\Bigg], \tag{27}$$

$$\begin{aligned}\frac{\partial^2 J_{BS}}{\partial \Delta_k \partial \Omega_k} &= \frac{\partial^2 J_{BS}}{\partial \Omega_k \partial \Delta_k} \\ &= -\Bigg(\tfrac{1}{2}\delta t \left(\cos\left(\tfrac{1}{2}\alpha\right) + \sin\left(\tfrac{1}{2}\alpha\right) r_x\right) \frac{\Delta_k}{\sqrt{\Omega_k^2+\Delta_k^2}} + \cos\left(\tfrac{1}{2}\alpha\right)\cos(\phi)\frac{\Delta_k\Omega_k}{\left(\Omega_k^2+\Delta_k^2\right)^{3/2}}\Bigg) \\ &\quad \times \Bigg(\tfrac{1}{2}\delta t \left(\cos\left(\tfrac{1}{2}\alpha\right) + \sin\left(\tfrac{1}{2}\alpha\right) r_x\right) \frac{\Omega_k}{\sqrt{\Omega_k^2+\Delta_k^2}} - \cos\left(\tfrac{1}{2}\alpha\right)\cos(\phi)\frac{\Delta_k^2}{\left(\Omega_k^2+\Delta_k^2\right)^{3/2}}\Bigg) \\ &\quad - \left(\sin\left(\tfrac{1}{2}\alpha\right) - \cos\left(\tfrac{1}{2}\alpha\right) r_x\right) \times \Bigg[- \tfrac{1}{2}\delta t \sin\left(\tfrac{1}{2}\alpha\right)\cos(\phi)\frac{\Omega_k^2\Delta_k}{\left(\Omega_k^2+\Delta_k^2\right)^2} \\ &\quad - \tfrac{1}{2}\delta t \left(\cos\left(\tfrac{1}{2}\alpha\right) + \sin\left(\tfrac{1}{2}\alpha\right) r_x\right)\frac{\Omega_k\Delta_k}{\left(\Omega_k^2+\Delta_k^2\right)^{3/2}} \\ &\quad + \tfrac{1}{2}\delta t \sin\left(\tfrac{1}{2}\alpha\right)\cos(\phi)\frac{\Delta_k^3}{\left(\Omega_k^2+\Delta_k^2\right)^2} \\ &\quad + \cos\left(\tfrac{1}{2}\alpha\right)\cos(\phi)\frac{\Delta_k^3-2\Delta_k\Omega_k^2}{\left(\Omega_k^2+\Delta_k^2\right)^{5/2}}\Bigg]. \end{aligned} \tag{28}$$

Based on SGD with parameter setting of ($\beta_1=\beta_2=\gamma_2=0, \gamma_1=1, \lambda=1$) in GADA method, the optimal control signals are depicted in figure (3 a_1, b_1) and the fidelity of gate optimization is depicted in figure (3 c_1). Also, with the GADA method, the optimal control signals are depicted in figure (3 a_2, b_2) and the fidelity of gate optimization is depicted in figure (3 c_2). The control signals are depicted in figure (3 a_2, b_2) and the fidelity of gate optimization is depicted in figure (3 c_2). After 23 samples of 1-microsecond control pulse we reach the fidelity of 0.9998 for beam-splitter gate optimization (see table 2) and the atomic beam-splitter gate at this optimal control reach:

$$U_{\text{atomBS}}(N\delta t) = \begin{pmatrix} 0.703-0.025i & 0.710i \\ 0.710i & 0.703+0.025i \end{pmatrix}, \quad N=23, \quad \delta t = 1\,\mu\text{s}. \tag{29}$$

By gate optimization, simultaneously we can control two populations of atoms, one population from state $|0\rangle$ to $|y+\rangle$ and other population from $|1\rangle$ to $|y-\rangle$ as we can see in figure (3 d_1) for SGD method and in figure (3 d_2) for GADA method.

Optimization Method	Control Pulse Number	Beam-Splitter Gate Fidelity
SGD	26	0.99985
AdaGrad	26	0.99991
LM	26	0.9999
GADA	23	0.99998
DADA	24	0.99996

Table 2 Fidelities and control parameters for different optimization methods.

4 Conclusion

Several researchers have developed and employed numerical optimal controls, such as SGD and AdaGrad, for quantum state preparation and some for gate synthesis. Here, we derived a general adaptive optimal methodology to speed up quantum gate realization and to increase the quantum gate fidelity. Several numerical optimizations can be deduced as a special case of our method; hence, we have more degrees of freedom to optimize the cost function of physical systems by this adaptive method. However, our optimal quantum control methodology was employed to realize atom interferometers; it will open up a new window for high-fidelity quantum gates realization for quantum computing purposes. For instance, we can realize the most important fundamental one-qubit gates such as NOT(σ_x), Hadamard ($\frac{1}{\sqrt{2}}(\sigma_x+\sigma_z)$), phase shift gate, etc. and also fundamental two-qubit gates such as CNOT ($|0\rangle\langle 0|\otimes \mathrm{I} + |1\rangle\langle 1|\otimes\sigma_x$), CPHASE ($|0\rangle\langle 0|\otimes \mathrm{I} + |1\rangle\langle 1|\otimes\sigma_z$), etc which are essential for quantum algorithms. In this research, we achieved

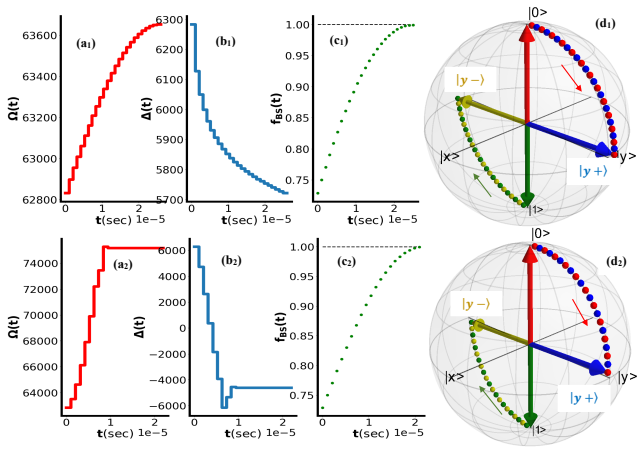

Fig. 3 Atom interferometer beam-splitter gate realization: Top is for SGD and Bottom is for GADA based on optimal quantum control methods. SGD parameters: $(\beta_1 = \beta_2 = \gamma_2 = 0, \gamma_1 = 1, \lambda = 1)$ and GADA parameters $(\beta_1 = 0.85, \beta_2 = 85, \gamma_1 = \gamma_2 = 1, \lambda = 10^{-1})$. (a_1, b_1) are the control pulses and (c_1) fidelity function for implementation of the atomic beam-splitter gate realization and (d_1) shows the simultaneous quantum state transfer $(|0\rangle \rightarrow \frac{1}{\sqrt{2}}(|0\rangle + i|1\rangle)$ and $\frac{1}{\sqrt{2}}(i|0\rangle + |1\rangle) \rightarrow |1\rangle$ on Bloch-sphere using optimal mirror gate realization with SGD. Figures (a_2, b_2, c_2) are the control pulses and the fidelity over time for mirror implementation with GADA. (d_2) displays simultaneous quantum state transfer using optimal beam-splitter gate realization on Bloch-sphere.

high fidelity of gate realization and faster convergence compared to conventional optimization methods. The method employed in this research is a promising methodology for quantum control applications from quantum sensing, quantum computing, and quantum simulations for different quantum system platforms such as superconductor circuits, atom spin systems and the spin quantum dot.

References

1. C.-W. Chou, D. B. Hume, T. Rosenband, D. J. Wineland, Science **329**, (2010)
2. X. Wu et al., Sci. Adv. **5**, (2019)
3. T. Kovachy et al., Nature **528**, (2015)
4. A. Loeb, D. Maoz, arXiv:1501.00996, (2015)
5. M. Abe et al., *Matter-wave Atomic Gradiometer Interferometric Sensor*, IOP Publishing (2021)
6. A. Arvanitaki, J. Huang, K. Van Tilburg, Phys. Rev. D, **91** (2015)
7. M.-S. Zhan et al., Int. J. Mod. Phys. D, **29,** (2020)
8. T. Kovachy et al., *Macroscopic scale atom interferometers: introduction, techniques, and applications*, Oxford University Press (2019)
9. J. Fang, J. Qin, Sensors, **12**, (2012)
10. T. L. Gustavson, Ph.D. thesis, Stanford University (2000)
11. J. Zhang, D. Burgarth, R. Laflamme, D. Suter, Phys. Rev. A **91**, (2015)
12. S. Kwon, A. Tomonaga, G. L. Bhai, S. J. Devitt, J.-S. Tsai, J. Appl. Phys., **129**, (2021)
13. P. Krantz et al. Appl. Phys. Rev., **6**, (2019)
14. H. Häffner, C. F. Roos, R. Blatt, Phys. Rep., **469**, (2008)
15. D. S. Weiss, M. Saffman, Phys. Today, **70**, (2017)
16. L. Henriet et al. Quantum, **4**, (2020)
17. G. M. Huang, T. J. Tarn, J. W. Clark, J. Math. Phys. **24**, (1983)
18. V. P. Belavkin, Autom. Remote Control, (1983)
19. W. S. Warren, H. Rabitz, M. Dahleh, Science, **259**, (1993)
20. S. Chu, Nature, **416**, (2002)
21. H. Robbins, S. Monro, Ann. Math. Stat., (1951)
22. H. B. McMahan, M. Streeter, Proc. 23rd Annu. Conf. Learn. Theory (COLT), (2010)
23. D. Zhou et al. Trans. Mach. Learn. Res. (2024)
24. N. Qian, Neural networks, **12**, (1999)
25. D. P. Kingma, J. Ba, Proc. 3rd Int. Conf. Learn. Represent. (ICLR) (2015)
26. Nelles, Oliver, *Nonlinear system identification*, IOP Publishing (2002)
27. M. D. Zeiler, arXiv:1212.5701, (2012)
28. Berman, Paul R, *Atom interferometry*, Academic press, (1997)
29. I. Glendinning, ResearchGate presentation, (2010)